Geophysical Research Letters

RESEARCH LETTER
10.1029/2018GL077877

Key Points:
- Cyclotron resonance of counterstreaming electrons is dominant for pitch angle scattering, consistent with quasi-linear theory
- Landau and cyclotron resonances are comparable for acceleration; here the energy source is the wave perpendicular electric field in both
- Substantial Landau parallel acceleration occurs with a finite wave-normal angle, even with negligible parallel electric field

Supporting Information:
- Supporting Information S1
- Movie S1
- Movie S2
- Movie S3
- Movie S4

Correspondence to:
C. L. da Silva,
caitano.dasilva@nmt.edu

Citation:
da Silva, C. L., Denton, R. E., Hudson, M. K., Millan, R. M., Liu, K., & Bortnik, J. (2018). Test-particle simulations of linear and nonlinear interactions between a 2-D whistler-mode wave packet and radiation belt electrons. *Geophysical Research Letters*, *45*, 5234–5245. https://doi.org/10.1029/2018GL077877

Received 21 MAR 2018
Accepted 7 MAY 2018
Accepted article online 11 MAY 2018
Published online 2 JUN 2018

Test-Particle Simulations of Linear and Nonlinear Interactions Between a 2-D Whistler-Mode Wave Packet and Radiation Belt Electrons

C. L. da Silva[1], R. E. Denton[2], M. K. Hudson[2], R. M. Millan[2], K. Liu[3], and J. Bortnik[4]

[1]Department of Physics and Langmuir Laboratory, New Mexico Institute of Mining and Technology, Socorro, NM, USA, [2]Department of Physics and Astronomy, Dartmouth College, Hanover, NH, USA, [3]Department of Physics, Auburn University, Auburn, AL, USA,
[4]Department of Atmospheric and Oceanic Sciences, University of California, Los Angeles, CA, USA

Abstract Using test-particle simulations, we describe (in 2-D) the interaction of an ensemble of electrons with a discrete whistler-mode wave packet, which propagates with a moderate wave-normal angle with respect to the background magnetic field. We evaluate both the average transport coefficients used in quasi-linear diffusion transport and also the full nonlinear wave-particle interactions. The magnitude of the calculated diffusion coefficients is found to increase proportionally to the wave amplitude squared, in agreement with quasi-linear diffusion theory. Cyclotron resonance of counterstreaming electrons ($n = 1$ harmonic number) is more important for pitch angle scattering than Landau resonance. Landau resonance of costreaming electrons ($n = 0$) is comparable to cyclotron resonance for energy diffusion and advection. Strong acceleration of high pitch angle, costreaming electrons arises in nonlinear wave-particle interactions with high-amplitude waves. In our simulations with zero parallel electric field, the energy source for electron acceleration is the wave's perpendicular electric field, in both the cyclotron and Landau resonances. The Landau resonance can happen even with zero parallel electric field, if the wave packet propagates with a finite wave-normal angle. This resonance between the particle's azimuthal velocity and the wave fields leads to trapping and substantial parallel acceleration.

Plain Language Summary We present a detailed analysis on how an individual plasma wave packet interacts with electrons trapped in the Earth's Van Allen radiation belts. The waves are in the so-called whistler mode, where both the wave fields and the electrons rotate around the background magnetic field lines at comparable frequencies, leading to substantial interaction between the two. In this investigation, we quantify both the average effect on a large group of particles and also the strong interactions that may happen with a selected few. Our results help quantifying how waves in the whistler mode contribute to the population balance of the radiation belts and especially how they can accelerate trapped electrons to high energies.

1. Introduction

Outside the plasmasphere, the Earth's magnetosphere is essentially a collisionless plasma, where the dynamic changes in the population balance are controlled by wave-particle interactions. Whistler-mode chorus is one of the most important wave types controlling the fluxes of the Earth's radiation belt electrons, because it can lead to both rapid local energization and loss of trapped electrons (Thorne, 2010). The electric and magnetic field fluctuations in these right-hand circularly polarized plasma waves rotate at an angular frequency ω in the same direction as electrons trapped in the radiation belts, and ω is a fraction of the electron gyrofrequency Ω_e. Additionally, their phase and group velocities are comparable to the parallel velocity of electrons in the hundreds of eV up to hundreds of keV energy ranges. All of these factors make chorus waves efficiently interact with trapped electrons and play a key role in the population balance of the radiation belts (Shprits et al., 2008; Thorne, 2010).

Basic linearization of the Vlasov equation indicates that the interaction between stochastic whistler-mode waves and electrons is significant only if the following resonance condition is met (Kennel & Engelmann, 1966):

$$\omega - k_{\parallel} v_{\parallel} = n\frac{\Omega_e}{\gamma} \tag{1}$$

where $n = 0, \pm1, \pm2, \ldots$. is the harmonic number, $k_{\parallel}$ is the parallel wave number, $v_{\parallel}$ is the electron parallel velocity, and $\gamma = 1/\sqrt{1 - v^2/c^2}$ is the Lorentz relativistic factor. For waves propagating nearly parallel to the background magnetic field, the dominant wave-electron interactions come from the $n = 1$ resonance. In the frame of reference moving with the electron's guiding center, the wave is doppler shifted to the relativistic gyrofrequency Ω_e/γ. For lower energies (where $\gamma < \Omega_e/\omega$) the $n = 1$ resonance is met for electrons counterstreaming with the waves, while for MeV energies the condition is met for costreaming electrons and waves.

Typically, wave-particle interactions in the Earth's radiation belts are characterized in the framework of quasi-linear diffusion theory (Albert, 2005; H. S. Fu et al., 2011, 2012; Summers, 2005; Summers et al., 1998). Quasi-linear diffusion theory is built on the fact that electrons interacting with low- to moderate-amplitude broadband waves undergo several small scatterings that collectively amount to diffusion in energy and pitch angle. The approach is to solve the Fokker-Planck equation, with diffusion coefficients dependent on the wave distribution, to obtain the evolution of the electron phase-space density (Summers, 2005). This strategy has been successful for describing long-term (>10 hr) changes in the radiation belt fluxes (Li et al., 2007; Thorne et al., 2013) but has failed to explain faster dynamics (Agapitov et al., 2015).

However, at sufficiently large wave amplitudes, wave-particle interactions can switch from stochastic to deterministic, giving rise to nonlinear phenomena that cannot be described by quasi-linear diffusion theory (Albert, 2002; Bortnik et al., 2008; Omura & Summers, 2006; Omura et al., 2007). One such example is particle phase trapping, where a particle is trapped by (and moves along with) the wave in a substantial fraction of its bounce orbit, leading to significant energy and/or pitch angle changes (see, e.g., Bortnik et al., 2008, Figure 2i). Besides high amplitude, other characteristics of chorus that correlate with nonlinear interactions are as follows: its discrete coherent (almost monochromatic) structure, frequency rising tone, and oblique propagation (Agapitov et al., 2014; Hsieh & Omura, 2017; Omura & Summers, 2006).

Test-particle simulations to characterize the role of nonlinear wave-particle interactions have usually been performed with 1-D models (where the spatiotemporal evolution of wave fields is prescribed along the magnetic field line) using either gyroaveraged equations of motion (Bortnik et al., 2008; Hsieh & Omura, 2017; Omura & Summers, 2006; Omura et al., 2007; Zheng et al., 2012) or Hamiltonian analysis (Agapitov et al., 2014; Albert, 2002; Artemyev et al., 2013). Some investigations have characterized wave-particle interactions between electrons and wave fields from self-consistent particle-in-cell (or hybrid) simulations but also often in 1-D (Hikishima et al., 2010; Katoh & Omura, 2007). A 2-D investigation in cartesian coordinates was undertaken by Drake et al. (2015).

In this work we characterize wave-particle interactions between electrons and a 2-D whistler-mode wave packet that is generated from a self-consistent simulation in a dipolar magnetic field geometry (da Silva et al., 2017; Wu et al., 2015). The wave fields are excited from temperature anisotropy of tens of keV ring-current electrons and are representative of lower band chorus. They form a discrete wave packet that evolves as a function of time and position along the field line and naturally has a finite perpendicular wavelength. We track an ensemble of electrons, distributed over all pitch angles and energies between 5 and 500 keV, as they interact with this discrete wave packet. We demonstrate that this approach can replicate key results from quasi-linear diffusion theory and also provide a detailed description of full nonlinear wave-particle interactions. We quantify the importance of cyclotron and Landau resonances for both pitch angle and energy diffusion, emphasizing the effects of increasing wave amplitude. We also describe the interaction of individual particles with the wave packet, demonstrating that the wave's perpendicular electric field can lead to energization in both Landau and cyclotron resonances.

2. Methodology

2.1. Hybrid Simulations of a Discrete Whistler-Mode Wave Packet

Two-dimensional simulations are performed using a hybrid fluid/particle-in-cell computer simulation model, which was first developed for investigations of electromagnetic ion cyclotron waves (Denton et al., 2014; Hu & Denton, 2009; Hu et al., 2010), and further extended to studies of whistler-mode waves (da Silva et al., 2017; Wu et al., 2015). The model treats the hot, anisotropic (i.e., ring current) electron population as particles, and the background (i.e., cold) electrons as an inertialess fluid. The total electron density (equal to the ion density) is 3.8 cm^{-3}, and the breakdown between hot (treated as particles), warm (particles), and cold (fluid) species is 6%, 10%, and 84%, respectively. The ratio between the plasma and cyclotron frequencies is $\omega_{pe}/\Omega_{e0} = 3.48$.

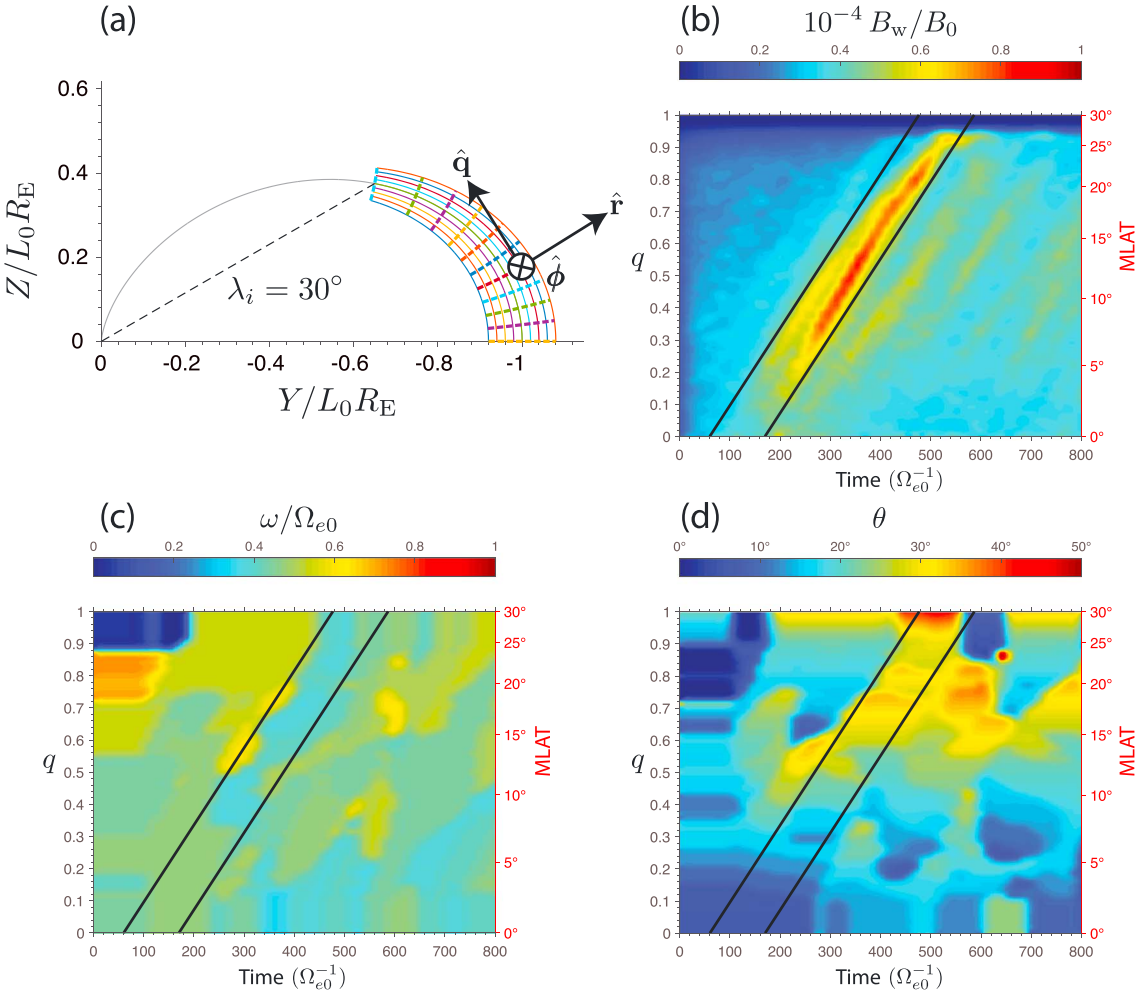

Figure 1. (a) The dipolar (q, r, ϕ) coordinate system used in this study, where q is a measure of length along the field line, $r = L/L_0$ is a normalized L shell, and ϕ is the azimuthal angle (into the plane). (b–d) Characteristics of the simulated whistler-mode waves as a function of position along field line and time. (b) Wave amplitude B_w. (c) Wave frequency ω. (d) Wave-normal angle θ. The wave frequency and wave-normal angle are calculated with a moving fast Fourier transform of the complex signal $S = B_{w,r} + iB_{w,\phi}$, along the central field line. The black lines are added to guide the eye to the region of highest wave power. In the right vertical axis we show the latitude at the central field line. MLAT = magnetic latitude.

The hot electrons have 15-keV parallel and 45-keV perpendicular temperatures. These input parameters are representative of observations (see, e.g., Fu et al., 2014). The detailed initial conditions of the simulations were presented in a previous publication (da Silva et al., 2017, Table 1 and Figure 4).

The background cold electron fluid population is evolved with electron MHD equations, while the particles respond to the Lorentz force. All equations are solved in a meridional plane in a coordinate system (q, r, ϕ) that follows the curvature of the Earth's dipolar magnetic field between the equator (where we apply a symmetry boundary condition) and 30° latitude (as shown in Figure 1a). Owing to limitations in computational resources, we simulate a system that is a factor of 12.8 times smaller than the region of interest at $L_0 = 5.5$. Although all other plasma parameters used here are realistic, the increased ratio between the Larmor radius and the magnetic field radius of curvature (by a factor of 12.8) introduces quantifiable effects in the analysis, which are discussed in section 3.

The plasma parameters listed above produce a high linear growth rate ($0.033\,\Omega_{e0}$) that produces waves with large amplitude. Thus, we rescale the wave amplitude to any desired value through a four-step technique. First, we calculate the background equilibrium magnetostatic field $\langle\vec{\mathbf{B}}\rangle_t$ through a time average, followed by k-space lowpass filtering. Second, a temporary wave field variable is defined as $\vec{\mathbf{B}}^*_w \equiv \vec{\mathbf{B}} - \langle\vec{\mathbf{B}}\rangle_t$. Third, the wave amplitude is rescaled as $\vec{\mathbf{B}}_w = \vec{\mathbf{B}}^*_w\ 10^{-4}/\max(B^*_{w,\phi})$, where in this case the desired wave amplitude

is $B_w = 10^{-4}B_0$, and $B^*_{w,\phi}$ is the component of $\vec{\mathbf{B}}^*_w$ in the $\hat{\boldsymbol{\phi}}$ direction (the magnetic field here is normalized to the equatorial value in the central L shell $B_0 = 180$ nT). Fourth, the total field is defined as $\vec{\mathbf{B}} = \vec{\mathbf{B}}_{dip} + \vec{\mathbf{B}}_w$, where $\vec{\mathbf{B}}_{dip}$ is the Earth's dipolar magnetic field. A similar scaling is done to the electric field, although it does not have an equilibrium component. In our simulations the high linear growth rate also appears to dominate over nonlinear growth processes that can cause rising tones; thus, the wave packet has approximately the same frequency content throughout the entire simulation time span (Figure 1c).

Figures 1b–1d show the characteristics of the generated whistler-mode wave packet: It is a discrete packet excited at the equator (compare Figure 1b to the coordinate system in Figure 1a); it is relatively broadband, with strong power in the frequency range between 0.3 and 0.5 Ω_{e0}, peaking at ~0.4 Ω_{e0}; the amplitude grows with time and latitude; the packet is initially almost parallel to the background magnetic field ($\theta \simeq 7°$); but as it propagates to higher latitudes, its wave-normal angle turns towards higher L shells (increasing up to ~40°).

2.2. Test-Particle Simulations

In order to characterize wave-particle interactions, test-particle simulations are performed with electrons traversing the whistler-mode wave packet shown in Figure 1. The test-particle initial distribution is uniform in energy from 5 to 500 keV, approximately uniform in equatorial pitch angle, and distributed evenly in the simulation domain (q, r). The test electrons are evolved using the relativistic Lorentz force equation:

$$\frac{d\vec{\mathbf{x}}}{dt} = \vec{\mathbf{v}}\,, \tag{2}$$

$$m\frac{d(\gamma\vec{\mathbf{v}})}{dt} = -e\left[\vec{\mathbf{E}}_w + \vec{\mathbf{v}} \times \left(\vec{\mathbf{B}}_{dip} + \vec{\mathbf{B}}_w\right)\right], \tag{3}$$

where $-e, m, \vec{\mathbf{x}}$, and $\vec{\mathbf{v}}$ are the particle's charge, mass, position, and velocity, while $\vec{\mathbf{E}}_w$, $\vec{\mathbf{B}}_w$, and $\vec{\mathbf{B}}_{dip}$ are the wave electric, wave magnetic, and background magnetostatic fields interpolated to the particle's position, respectively. The position and velocity of over 7 million particles are tracked using the Boris algorithm (Birdsall & Langdon, 1985, pp. 61–63). Equations (2)–(3) are solved in 3-D Cartesian coordinates (x, y, z) with fields rotated from the hybrid code curvilinear coordinates to avoid effects of fictitious forces due to the curved frame of reference (q, r, ϕ).

To investigate the efficiency of this wave packet in causing pitch angle scattering and acceleration of radiation belt electrons, we calculate the pitch angle and energy diffusion coefficients, respectively, as

$$D_{\alpha\alpha} \equiv \frac{\langle \Delta\alpha^2_{eq} \rangle}{2\Delta t}\,, \quad D_{KK} \equiv \frac{\langle \Delta K^2 \rangle}{2\Delta t}\,, \tag{4}$$

and also the respective advection coefficients as

$$A_\alpha \equiv \frac{\langle \Delta\alpha_{eq} \rangle}{\Delta t}\,, \quad A_K \equiv \frac{\langle \Delta K \rangle}{\Delta t}\,, \tag{5}$$

where $\Delta\alpha_{eq}$ is the change in equatorial pitch angle $\alpha_{eq} = \cos^{-1}(\sqrt{1 - v_\perp^2 B_{eq}/v^2 B})$ and ΔK is the change in energy $K = (\gamma - 1)mc^2$, where v and $v_\perp$ are the particle's total and perpendicular velocities, respectively, while c is the speed of light in vacuum. Following Anderson et al. (1997), we evaluate the local and equatorial magnetic fields, B and B_{eq}, at the particle's guiding center position. The average $\langle\ \rangle$ is performed over binned particles of similar initial α_{eq} and K. Since the electrons are distributed all over the meridional plane in L and magnetic latitude (MLAT), the coefficients defined above represent bounce-averaged values. The coefficients D_{ii} and A_i, in the ith direction, as defined in equations (4)–(5) are the transport coefficients appearing in the Fokker-Planck equation. The A_i coefficients may be best interpreted as a measure of the total distribution drift in velocity space, which also has a contribution arising from the gradient of the diffusion coefficient.

3. Results and Discussion

The test particles traverse the whistler-mode wave fields generated from a self-consistent simulation but rescaled to have maximum amplitudes between 10^{-4} and $10^{-1}B_0$, ranging from typical amplitudes observed

in the Earth's magnetosphere (e.g., Li et al., 2011) to some of the highest amplitudes observed (e.g., Cattell et al., 2008; Wilson et al., 2011). We have evaluated the inhomogeneity ratio R (Omura et al., 2007, equation (11); Albert & Bortnik, 2009, equation (5)) for our simulation parameters. A value $|R| < 1$ indicates conditions where nonlinear wave-particle interactions may arise (Albert & Bortnik, 2009). The wave amplitudes chosen in this paper are such that for $B_w = 10^{-4}B_0$, $|R| \gg 1$ (i.e., fully linear dynamics), while for $B_w = 10^{-1}B_0$, $|R| \ll 1$ (i.e., prone to nonlinear behavior), for most values of equatorial pitch angle in the energy range studied. The amplitude $B_w = 10^{-2}B_0$ represents an intermediate scenario where only particles with high equatorial pitch angles may display nonlinear behavior.

The first two rows in Figure 2 show the calculated pitch angle (a–d) and energy (e–h) diffusion coefficients. The lower/upper half of each panel shows costreaming/counterstreaming electrons, as labeled in the right vertical axis. From left to right, the reader can see the effect of increasing wave amplitude, from 10^{-4} (a, e) to 10^{-2} (b, c, f, g) and finally to $10^{-1}B_0$ (d, h). The color scale is proportional to B_w^2, making panels (b) through (d) and (e) through (h) look similar, as predicted by quasi-linear diffusion theory (e.g., Summers, 2005). The exception is panel (a), for reasons discussed below. It is easy to see, by comparing $D_{\alpha\alpha}$ in panels (a)–(d) with the overlaid resonance curves, that pitch angle diffusion is largely dominated by the $n = 1$ (cyclotron) and $n = 0$ (Landau) resonances. The resonance curves are calculated using equation (1), assuming that waves propagate with a constant frequency $\omega = 0.4\Omega_{e0}$, with the wave number k varying according to a cold plasma linear dispersion equation, and assuming that the wave-normal angle evolves as $\theta \simeq 7° + 0.65\times$ MLAT, which is a linear fit to the trend shown in Figure 1d (we note that a similar linear trend has also been inferred from chorus statistical analysis, but with a different proportionality coefficient $\theta \approx 2\times$ MLAT; Agapitov et al., 2013). In panels (b) and (f), the resonance curves emphasize the effect of MLAT, showing that the dominant interactions happen for $n = 0, 1$ between 0° and 20° latitude.

In Figure 2, panels (a), (b), (e), and (f) on the left and (c), (d), (g), and (h) on the right show the effect of selecting a longer and shorter time range Δt for calculation of diffusion coefficients, respectively. By contrasting panels (b) and (c) we can see that the high-diffusion patches for costreaming electrons in panel (b) (located at around $\alpha_{eq} \approx 60°$ and $K = 100–200$ keV, and close to 0° and 50–150 keV) disappear in panel (c) where a shorter time interval is used. Detailed analysis of individual particle trajectories shows that the two patches in panel (b) result from particles that are initially propagating poleward, reflect towards the equator by the magnetic mirror force, and interact with the waves via counterstreaming cyclotron resonance. This effect is reduced using a shorter time interval, as shown in panel (c). In panels (c), (d), (g), and (h) we show the resonance curves for $n = -1, 0, 1, 2$ at a selected latitude (MLAT = 7.5°) where the peak wave power is approximately located in the time interval 250–300 Ω_{e0}^{-1}. Once more, the comparison between the resonance curves and diffusion coefficients shows that wave-particle interactions are largely dominated by the first cyclotron and Landau resonances.

One prominent feature in Figures 2a and 2c that does not align with the resonance curves can be seen in the top- and bottom-right corners. The high pitch angle diffusion rate in those two regions is due to a combination of the enhanced curvature of our system (because we simulate a 12.8-times scaled-down version of the magnetosphere) and the short simulation time. Going from left to right in Figure 2, we can see that the relatively high diffusion in those two regions is alleviated by both increasing Δt and the wave amplitude. The reason why this effect arises for particles with high energy and low pitch angle (i.e., high parallel velocity) is well captured by the parameter η, described by Anderson et al. (1997, equation (3)). The parameter $\eta = 2\pi v_{\parallel}\gamma/\Omega_e/R_c$ is the ratio between the parallel distance travelled along the field line in one gyroperiod ($2\pi v_{\parallel}\gamma/\Omega_e$) and the radius of curvature of the magnetic field (R_c). The higher η is, the more likely we are to see the onset of nonadiabatic particle motion giving rise to field-line curvature scattering (Anderson et al., 1997; Young et al., 2002). Note that $\eta = 2\pi\varepsilon\cot(\alpha_{eq}) \propto \varepsilon$, where $\varepsilon = \rho_L/R_c$ is the more familiar ratio between the Larmor radius (ρ_L) and the radius of curvature of the magnetic field. The nonresonant diffusion shown in the bottom- and top-right corners of Figures 2a and 2c is due to the neglect of higher-order terms in the first adiabatic invariant (Young et al., 2002, equations (A1)–(A2)), which are stronger when η is large. These numerical errors are illustrative of the effects of choosing different test-particle simulation intervals Δt: With a longer Δt one could track the particles to their mirror points and evaluate α_{eq} with minimal error (e.g., Anderson et al., 1997), but equations (4)–(5) only represent Fokker-Planck transport coefficients in the limit that Δt is small. Remarkably, these inaccuracies do not result in energy changes, as shown in panels (e)–(h). We have performed

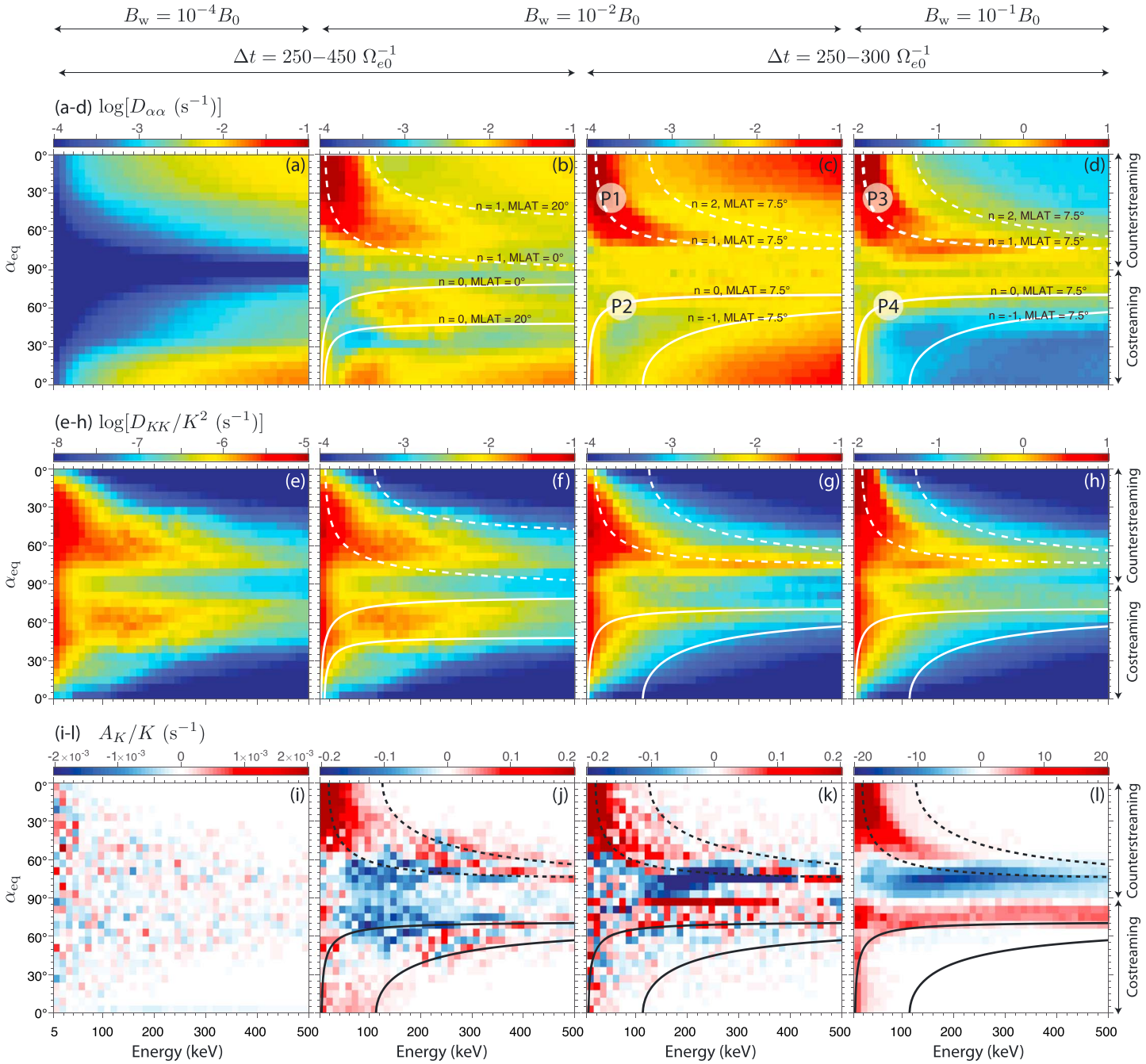

Figure 2. Pitch angle diffusion (a–d), energy diffusion (e–h), and energy advection (i–l) coefficients as a function of equatorial pitch angle and kinetic energy. Wave amplitudes are 10^{-4} (a, e, i), 10^{-2} (b, c, f, g, j, k), and $10^{-1}B_0$ (d, h, l). Simulation time interval spans 250 to 450 Ω_{e0}^{-1} (a, b, e, f, i, j) and 250 to 300 Ω_{e0}^{-1} (c, d, g, h, k, l). The overlaid curves mark the resonance condition calculated from equation (1) and are labeled according to harmonic number (n) and magnetic latitude (MLAT). See text for details. Vertically aligned panels have the same wave amplitude, simulation time interval, and resonance curves.

a simulation run without the wave fields (i.e., $B_w = 0$, shown in the supporting information Figure S3), which produces a finite $D_{\alpha\alpha}$ equivalent to the one shown in Figure 2a, but no energy diffusion ($D_{KK} = 0$). This demonstrates that the effects described in this paragraph are not attributed to the wave fields.

The striking similarity between panels (e)–(h) in Figure 2 indicates that the energy diffusion coefficients scale as $\propto B_w^2$, as predicted by quasi-linear diffusion theory (e.g., Summers, 2005). Energy diffusion is comparable for both costreaming and counterstreaming particles, while pitch angle diffusion is significantly more important

in the latter case. Averaging over the energy range shown in Figure 2 reveals that pitch angle diffusion peaks at 0° for counterstreaming particles. Contrastingly, energy diffusion is maximum at ∼60°, with two comparable peaks for costreaming and counterstreaming particles, where the ($n = 0, 1$) resonance curves become horizontal, that is, become weakly dependent on energy. Averaging over pitch angles reveals the trend that, at high energies, diffusion coefficients $D_{\alpha\alpha}$ and D_{KK}/K^2 decrease as $\propto 1/\gamma^2$, also in agreement with quasi-linear diffusion theory (comparing to equations (17) and (19) of Summers, 2005).

We have also calculated advection coefficients according to equation (5). Panels (i)–(l) in Figure 2 show the energy advection A_K/K, indicating that, on average, counterstreaming particles above/below the $n = 1$ resonance curve and costreaming particles above/below the $n = 0$ resonance curve are accelerated/decelerated. Regarding pitch angle changes (the pitch angle advection coefficient is not shown for the sake of brevity, but see Figure S5), we obtain the intuitive result that particles close to 90° have reducing pitch angles, while counterstreaming particles above the $n = 1$ and costreaming below the $n = 0$ resonance curves have increasing pitch angles. These advective pitch angle and energy changes tend to transport the particles towards the resonance curve (see also Liu et al., 2012), which further increases advection rates in a nonlinear feedback process. Note that quasi-linear theory predicts that the advection coefficients shown in Figures 2i and 2j should be qualitatively similar to each other and only differ by a constant multiplying factor $\propto B_w^2$, similar to the diffusion coefficients shown in Figures 2e and 2f. Nonetheless, we find that at low wave amplitudes, there is no advection and the calculated coefficient is dominated by particle noise (Figure 2i), while at high wave amplitudes, there is strong advection for particles near the resonance curves (Figure 2l). We attribute this result to the nonlinear feedback mechanism described above, with an important consequence being the strong acceleration of costreaming electrons with high equatorial pitch angles (see Figure 2l).

According to Albert (2002), the energy changes arising from phase bunching have the same sign as $-dB/dq$, where q is the coordinate position along the magnetic field line. For wave packets starting at the equator and propagating to higher latitudes, such as in our simulation, the energy changes should be negative. Albert (2002) also asserts that, typically, particles with large pitch angle and low energy are prone to experiencing phase bunching. These two points combined have led us to interpret the blue patch in Figure 2l as due to phase bunching. On the other hand, the positive energy changes for costreaming particles with high equatorial pitch angle, in the same figure, are attributed to phase trapping and are discussed in detail below in context of the panel P4 of Figure 3. An attempt to estimate the linear and nonlinear contributions to the total advection coefficient is made on the supporting information manuscript.

To better understand the wave-particle interactions, we have analyzed individual particle trajectories. We selected two particles from the data in Figure 2d ($B_w = 10^{-1}B_0$), each having the highest $|\Delta\alpha_{eq}|$ in the regions marked as P3 and P4. We also ran these particles through lower-amplitude waves ($B_w = 10^{-2}B_0$), marked as P1 and P2 in Figure 2c. The temporal evolution of parameters associated with these four particles is shown in Figure 3 in panels labeled P1–P4. The subpanels show the (a) equatorial pitch angle α_{eq} with scale on the left vertical axis and energy with scale on the right, (b) components of wave magnetic field B_w, (c) wave electric field E_w, and (d) rate of energy gain $\vec{\mathbf{v}} \cdot \vec{\mathbf{F}}$ with scale on the left axis and perpendicular velocity $v_\perp = \sqrt{v_r^2 + v_\phi^2}$ with scale on the right. Subpanels (e, f, g) show the forces (F_q, F_r, F_ϕ) with scale on the left vertical axis and velocities (v_q, v_r, v_ϕ) with scale on the right in the ($\hat{\mathbf{q}}, \hat{\mathbf{r}}, \hat{\boldsymbol{\phi}}$) directions, respectively. The curvilinear coordinate system (q, r, ϕ) is shown in Figure 1a. The fields B_w and E_w are expressed in units of $10^{-3}B_0$ and $10^{-3}cB_0$, respectively. The rate of energy gain is expressed in units of $10^{-3}ec^2B_0$. The forces are expressed in units of $10^{-3}ecB_0$, and the velocities in terms of c. We also show the net energy gain and the net force as a yellow solid area in the background of subpanels (d) and (e–g), respectively.

Particles/panels P1 and P3 in Figure 3 show the cyclotron resonance. Particles P1 and P3 propagate towards the equator; their initial and final latitudes are shown in subpanels (a). It is easy to see in panels P1f and P1g that the particle's perpendicular velocity components, v_r and v_ϕ, resonate with the forces (in Lorentz equation (3)) pointing in those respective directions during the interval $t = 250$ to $270\Omega_{e0}^{-1}$. The resonance condition is met because the particle is counterstreaming against the wave propagation direction at sufficiently low velocity such that, in the Lagrangian frame of reference, the wave frequency is doppler shifted up to the cyclotron frequency. During this interval, the perpendicular electric field acts as an energy source for the acceleration (panel P1d). The magnetic force from the wave tends to reduce parallel velocity (panel P1e) and increase the perpendicular one (P1f and P1g). The net effect is perpendicular acceleration that leads to α_{eq} and K increasing concurrently (P1a). The difference for particle P3 (with a stronger wave amplitude) is that the interaction

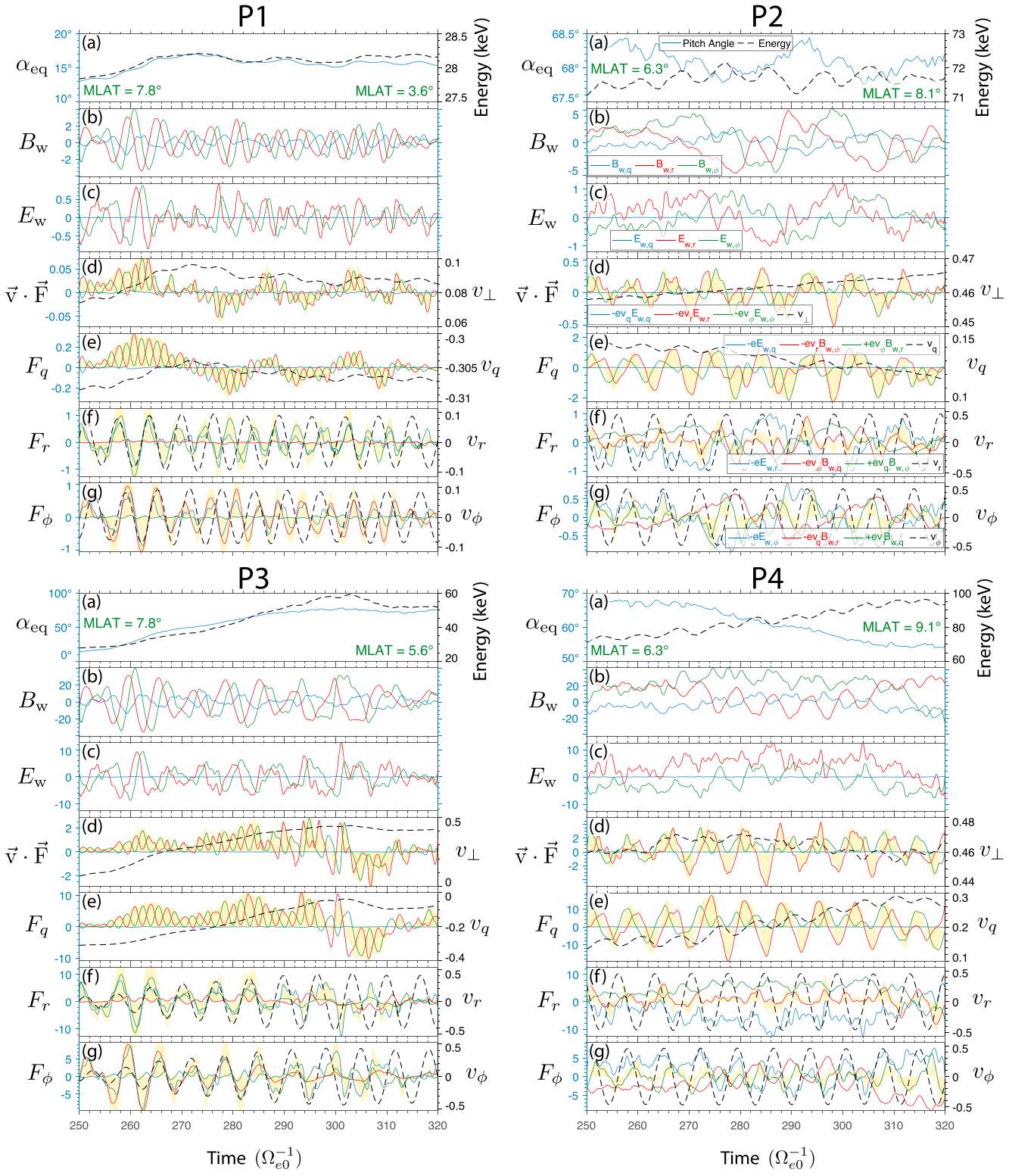

Figure 3. Panels P1–P4 show the temporal evolution of several quantities for four selected particles. The subpanels show (a) equatorial pitch angle α_{eq} and energy, (b) components of wave magnetic field B_w, (c) wave electric field E_w, and (d) rate of energy gain $\vec{\mathbf{v}} \cdot \vec{\mathbf{F}}$ and perpendicular velocity $v_\perp$. Subpanels (e, f, g) show the forces (F_q, F_r, F_ϕ) and velocities (v_q, v_r, v_ϕ) in the ($\hat{\mathbf{q}}, \hat{\mathbf{r}}, \hat{\boldsymbol{\phi}}$) directions, respectively. See text for units of quantities in subpanels (b–g). Solid lines correspond to the left-side vertical axis, while dashed lines correspond to the right-side axis. The keys to the line colors and styles are given in panel P2 and are the same in the four panels.

lasts longer, up to $t = 300\,\Omega_{e0}^{-1}$ (panels P3f and P3g). This happens because the parallel deceleration due to the wave force F_q is strong enough to compensate for the mirror force, the velocities v_r and v_ϕ get locked to the wave phase (the phase trapping can be seen in panels P3f and P3g), and the particle is decelerated almost to a stop (panel P3e).

This publication is accompanied by four supporting information movie animations (Movies S1–S4) that show the electrons P1–P4 propagating through the whistler-mode wave fields. These movies aid the visualization of the wave-particle interactions described in the context of Figure 3. Please refer to the accompanying supporting information manuscript for a detailed description of the movies.

Particles/panels P2 and P4 in Figure 3 show the Landau resonance. Particles P2 and P4 propagate towards the pole; their initial and final latitudes are listed in subpanels (a). Particle P2 and the wave packet are costreaming at approximately the same velocity, which causes the particle to "see" roughly constant wave fields (panels P2b and P2c, during the first ~3 gyroperiods). This brief interaction leads to a small reduction in equatorial pitch angle and increase in energy (panel P2a) due to a net parallel force (panel P2e). The net parallel force is not strong enough to counterbalance the mirror force and v_q decreases during the interaction interval (panel P2e). The difference for particle P4 (with a stronger wave amplitude) is that the particle is dragged along by the wave packet. As both particle and wave packet reach higher latitudes, the wave overtakes the particle because its phase velocity increases roughly as $\propto \sqrt{B/B_0}$ and the mirror force tends to reduce the particle's parallel velocity as $\propto \sqrt{1-\sin^2(\alpha_{eq})B/B_0}$. As particle P4 starts to lag behind, and the particle's guiding center position aligns with a zero value of the wave field, a new feature of the Landau resonance arises, which is only possible due to the finite wave-normal angle (or finite component of wave vector $k_\perp$). When the particle P4's guiding center is in Landau resonance with a wave node, and the wave fronts are tilted with respect to the parallel direction $\hat{\mathbf{q}}$, there is automatically a resonance of the azimuthal velocity (v_ϕ) of the particle at the radial limits of the gyromotion with the azimuthal electric field (as shown in panel P4g), responsible for energization (P4d, green line), and the radial magnetic field, responsible for dragging the particle along (P4e, green line). The particle trapping lasts up to $t = 310\,\Omega_{e0}^{-1}$, amounting to significant parallel acceleration, which is reflected in the energy gain and pitch angle decrease shown in panel P4a.

Figure 4 and Movie S4 further illustrate this interaction. Figure 4 shows particle P4's trajectory overlaid on the wave fields. The Landau-$k_\perp$ resonant acceleration shown in Figure 4 is self-induced by the gyromotion. If a resonant particle's gyrocenter remains at a node of the azimuthal electric field and radial magnetic field, the particle's azimuthal velocity will automatically resonate with those wave field components as long as there is a finite $k_\perp$ value. The interaction is optimal if the perpendicular wavelength is $\sim 4\rho_L$, where ρ_L is the relativistic electron gyroradius, but also occurs if the perpendicular wavelength is larger. This assertion can also be understood from analysis of the gyroaveraged equations of motion. From equation (A7) in Liu et al. (2011), the quasi-linear pitch angle diffusion coefficient due to Landau resonance comes from two parts: one proportional to $E_\perp J_1$ and another proportional to $E_\parallel J_0$, here $E_\parallel = E_{w,q}$ and $E_\perp = \sqrt{E_{w,r}^2 + E_{w,\phi}^2}$. The argument of the Bessel functions J_1 and J_0 is $k_\perp \rho_L$. So, if $E_\parallel$ is zero, the transverse electric field can still contribute to the scattering when $k_\perp$ is not zero. The scattering peaks when J_1 peaks. The first peak of J_1 occurs when $k_\perp \rho_L \approx 1.8$. This leads to an optimal perpendicular wavelength of $(2\pi/1.8)\rho_L \approx 3.5\rho_L$. This number is close to the $4\rho_L$ estimate above. However, the net effect of the interaction is complex due to particle trapping at the resonance, as discussed below.

It can be seen from Figures 4a and 4b that v_ϕ has the same sign as $B_{w,r}$ on both sides of the particle's orbit, leading to a net force $ev_\phi B_{w,r}$ pointing in the $+\hat{\mathbf{q}}$ direction, which is responsible for dragging the particle along with the packet. At the same time, the particle is energized. The energy source for the acceleration is the wave perpendicular electric field, as is evident in Figures 4c and 4d because v_ϕ and $E_{w,\phi}$ have opposite signs on both sides of the orbit (thus, $\vec{\mathbf{v}} \cdot \vec{\mathbf{F}}_\phi = -ev_\phi E_{w,\phi}$ is positive). The net effect is particle trapping at the resonance and strong parallel acceleration. This parallel acceleration can cause precipitation into the atmosphere of energetic electrons that are initially far from the loss cone. The precipitation happens in the same hemisphere as the waves and correlates temporally with the lifetime of the wave packet. This mechanism may contribute in part to explain the origin of the short-lived (i.e., bursty), tens to hundreds of keV energetic precipitation, known as microbursts (Millan & Thorne, 2007, and references therein). This type of resonant interaction is important in magnetosonic waves, which propagate quasi-perpendicular to the magnetic field line and only interact with electrons via Landau resonance (Liu et al., 2011). A similar interaction could also occur for equatorially trapped

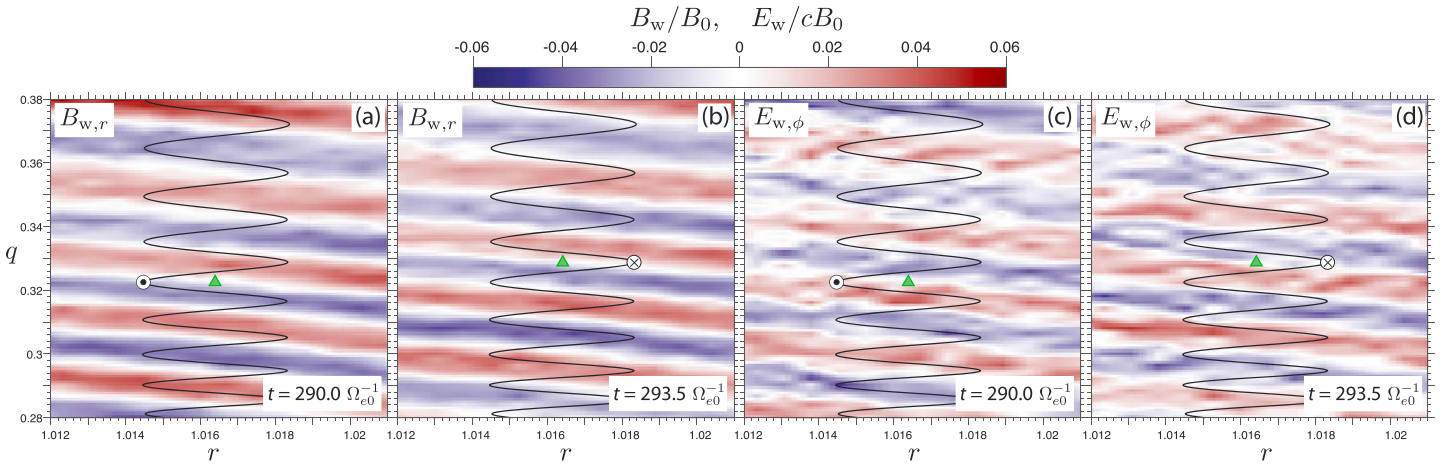

Figure 4. Landau-$k_\perp$ resonance experienced by particle P4. Wave $B_{w,r}$ (a, b) and $E_{w,r}$ (c, d) fields at two different time instants $t = 290.0\Omega_{e0}^{-1}$ (a, c) and 293.5 Ω_{e0}^{-1} (b, d), about a half gyroperiod apart. The solid black line shows the total particle trajectory in the q-r plane. The circle and the triangle mark the instantaneous position of the particle and guiding center, respectively. A circle with a dot (⊙) indicates that the particle's v_ϕ velocity points out of the page, while a circle with a cross (⊗) indicates that the particle is moving into the page.

($\alpha_{eq} \approx 90°$) electrons interacting with ion scale (effectively zero frequency) waves like electromagnetic ion cyclotron waves, as long as the wave has finite amplitude and a perpendicular component of the wave vector at the magnetic equator. This cannot occur using the symmetry boundary conditions that we have used in this paper but could occur if that boundary condition is relaxed.

In our hybrid model the electromagnetic fields are evaluated from electron MHD equations (da Silva et al., 2017, equations (1)–(3)). The electric field is obtained from a simplified Ohm's law involving the cold electron population velocity $\vec{\mathbf{u}}_{ec}$, $\vec{\mathbf{E}}_w = -\vec{\mathbf{u}}_{ec} \times (\vec{\mathbf{B}}_{dip} + \vec{\mathbf{B}}_w)$, which predicts that the parallel electric field $E_{w,q}$ is very small, even when waves are propagating with a finite wave-normal angle. This feature is evident in subpanels (c) of Figure 3. Therefore, in the present work, the energization of all particles, shown in subpanels (d), results from the wave's perpendicular electric field, and the changes in velocity in the parallel direction are entirely due to the wave's perpendicular magnetic field components. According to Figure 3, the described dynamics leads to parallel deceleration/acceleration in the cyclotron/Landau resonance cases. It is common practice in the whistler-mode wave literature to characterize the effects of the Landau resonance in terms of the parallel electric field (e.g., Agapitov et al., 2015; Artemyev et al., 2013). However, it can be seen from the present work and even from analysis using the gyroaveraged equations that the wave's perpendicular electric field (at moderate wave-normal angles) plays a key role in electron energization via Landau resonance (e.g., Hsieh & Omura, 2017, section 4.1; Liu et al., 2011, equation (A7); Shklyar & Matsumoto, 2009, equation (3.46)).

4. Summary

In this paper, we presented test-particle simulations in which an ensemble of electrons, covering all pitch angles and energies between 5 and 500 keV, interacts with a 2-D whistler-mode wave packet; such an approach can retrieve both average transport coefficients used in quasi-linear diffusion theory and also the full nonlinear wave-particle interactions. The magnitude of the calculated diffusion coefficients is found to increase proportionally to the wave amplitude squared, in agreement with quasi-linear diffusion theory. However, strong energy advection arises with increasing wave amplitude, evidencing an important nonlinear effect. Cyclotron resonance of counterstreaming electrons ($n = 1$ harmonic number) is more important for pitch angle scattering than Landau resonance. Landau resonance of costreaming electrons ($n = 0$) is comparable to cyclotron resonance for energy diffusion and advection. The energy source for electron acceleration is the wave's perpendicular electric field in both the cyclotron and Landau resonances. Finally, we thoroughly described how intense Landau parallel acceleration can happen even with zero parallel electric field.

Acknowledgments
This research was supported by NSF AGS-1155934 and AGS-1602469 and NASA NNX13AD65G grants to Dartmouth College. This work was also supported by JHU/APL under NASA contracts NNN16AA09T and NNN06AA01C to UMN and UNH with subcontracts to Dartmouth. C. L. da Silva is thankful for the support from the Society of Fellows at Dartmouth College and the Department of Physics at New Mexico Tech. The work of K. Liu at Auburn University was supported by NASA grants NNX16AM98G and NNX17AI52G. J. Bortnik would like to acknowledge the support from the NSF/DOE basic plasma physics award DE-SC0010578 and NASA grant NNX16AG21G. We are thankful for discussions with Shawn Young. Simulation data shown in this manuscript are publicly available at Zenodo (da Silva et al., 2018).

References

Agapitov, O., Artemyev, A., Krasnoselskikh, V., Khotyaintsev, Y. V., Mourenas, D., Breuillard, H., et al. (2013). Statistics of whistler mode waves in the outer radiation belt: Cluster STAFF-SA measurements. *Journal of Geophysical Research: Space Physics*, *118*, 3407–3420. https://doi.org/10.1002/jgra.50312

Agapitov, O. V., Artemyev, A. V., Mourenas, D., Krasnoselskikh, V., Bonnell, J., Contel, O. L., et al. (2014). The quasi-electrostatic mode of chorus waves and electron nonlinear acceleration. *Journal of Geophysical Research: Space Physics*, *119*, 1606–1626. https://doi.org/10.1002/2013JA019223

Agapitov, O. V., Artemyev, A. V., Mourenas, D., Mozer, F. S., & Krasnoselskikh, V. (2015). Nonlinear local parallel acceleration of electrons through Landau trapping by oblique whistler mode waves in the outer radiation belt. *Geophysical Research Letters*, *42*, 10,140–10,149. https://doi.org/10.1002/2015GL066887

Albert, J. M. (2002). Nonlinear interaction of outer zone electrons with VLF waves. *Geophysical Research Letters*, *29*(8), 1275. https://doi.org/10.1029/2001GL013941

Albert, J. M. (2005). Evaluation of quasi-linear diffusion coefficients for whistler mode waves in a plasma with arbitrary density ratio. *Journal of Geophysical Research*, *110*, A03218. https://doi.org/10.1029/2004JA010844

Albert, J. M., & Bortnik, J. (2009). Nonlinear interaction of radiation belt electrons with electromagnetic ion cyclotron waves. *Geophysical Research Letters*, *36*, L12110. https://doi.org/10.1029/2009GL038904

Anderson, B. J., Decker, R. B., Paschalidis, N. P., & Sarris, T. (1997). Onset of nonadiabatic particle motion in the near-Earth magnetotail. *Journal of Geophysical Research*, *102*(A8), 17,553–17,569. https://doi.org/10.1029/97JA00798

Artemyev, A. V., Vasiliev, A. A., Mourenas, D., Agapitov, O. V., & Krasnoselskikh, V. V. (2013). Nonlinear electron acceleration by oblique whistler waves: Landau resonance vs. cyclotron resonance. *Physics of Plasmas*, *20*(122901). https://doi.org/10.1063/1.4836595

Birdsall, C. K., & Langdon, A. B. (1985). *Plasma physics via computer simulation*. New York: McGraw-Hill.

Bortnik, J., Thorne, R. M., & Inan, U. S. (2008). Nonlinear interaction of energetic electrons with large amplitude chorus. *Geophysical Research Letters*, *35*, L21102. https://doi.org/10.1029/2008GL035500

Cattell, C., Wygant, J. R., Goetz, K., Kersten, K., Kellogg, P. J., von Rosenvinge, T., et al. (2008). Discovery of very large amplitude whistler-mode waves in Earth's radiation belts. *Geophysical Research Letters*, *35*, L01105. https://doi.org/10.1029/2007GL032009

da Silva, C. L., Denton, R. E., Hudson, M. K., Millan, R. M., Liu, K., & Bortnik, J. (2018). Simulation data output used in test-particle simulations of linear and nonlinear interactions between a 2D whistler-mode wave packet and radiation belt electrons, Zenodo, Dataset. https://doi.org/10.5281/zenodo.1205074

da Silva, C. L., Wu, S., Denton, R. E., Hudson, M. K., & Millan, R. M. (2017). Hybrid fluid-particle simulation of whistler-mode waves in a compressed dipole magnetic field: Implications for dayside high-latitude chorus. *Journal of Geophysical Research: Space Physics*, *122*, 432–448. https://doi.org/10.1002/2016JA023446

Denton, R. E., Jordanova, V. K., & Fraser, B. J. (2014). Effect of spatial density variation and O^+ concentration on the growth and evolution of electromagnetic ion cyclotron waves. *Journal of Geophysical Research: Space Physics*, *119*, 8372–8395. https://doi.org/10.1002/2014JA020384

Drake, J. F., Agapitov, O. V., & Mozer, F. S. (2015). The development of a bursty precipitation front with intense localized parallel electric fields driven by whistler waves. *Geophysical Research Letters*, *42*, 2563–2570. https://doi.org/10.1002/2015GL063528

Fu, H. S., Cao, J. B., Mozer, F. S., Lu, H. Y., & Yang, B. (2012). Chorus intensification in response to interplanetary shock. *Journal of Geophysical Research*, *117*, A01203. https://doi.org/10.1029/2011JA016913

Fu, H. S., Cao, J. B., Yang, B., & Lu, H. Y. (2011). Electron loss and acceleration during storm time: The contribution of wave-particle interaction, radial diffusion, and transport processes. *Journal of Geophysical Research*, *116*, A10210. https://doi.org/10.1029/2011JA016672

Fu, X., Cowee, M. M., Friedel, R. H., Funsten, H. O., Gary, S. P., & Hospodarsky, G. B. (2014). Whistler anisotropy instabilities as the source of banded chorus: Van Allen Probes observations and particle-in-cell simulations. *Journal of Geophysical Research: Space Physics*, *119*, 8288–8298. https://doi.org/10.1002/2014JA020364

Hikishima, M., Omura, Y., & Summers, D. (2010). Microburst precipitation of energetic electrons associated with chorus wave generation. *Geophysical Research Letters*, *37*, L07103. https://doi.org/10.1029/2010GL042678

Hsieh, Y.-K., & Omura, Y. (2017). Nonlinear dynamics of electrons interacting with oblique whistler mode chorus in the magnetosphere. *Journal of Geophysical Research: Space Physics*, *122*, 675–694. https://doi.org/10.1002/2016JA023255

Hu, Y., & Denton, R. E. (2009). Two-dimensional hybrid code simulation of electromagnetic ion cyclotron waves in a dipole magnetic field. *Journal of Geophysical Research*, *114*, A12217. https://doi.org/10.1029/2009JA014570

Hu, Y., Denton, R. E., & Johnson, J. R. (2010). Two-dimensional hybrid code simulation of electromagnetic ion cyclotron waves of multi-ion plasmas in a dipole magnetic field. *Journal of Geophysical Research*, *115*, A09218. https://doi.org/10.1029/2009JA015158

Katoh, Y., & Omura, Y. (2007). Relativistic particle acceleration in the process of whistler-mode chorus wave generation. *Geophysical Research Letters*, *34*, L13102. https://doi.org/10.1029/2007GL029758

Kennel, C. F., & Engelmann, F. (1966). Velocity space diffusion from weak plasma turbulence in a magnetic field. *Physics of Fluids*, *9*(12), 2377–2388. https://doi.org/10.1063/1.1761629

Li, W., Bortnik, J., Thorne, R. M., & Angelopoulos, V. (2011). Global distribution of wave amplitudes and wave normal angles of chorus waves using THEMIS wave observations. *Journal of Geophysical Research*, *116*, A12205. https://doi.org/10.1029/2011JA017035

Li, W., Shprits, Y. Y., & Thorne, R. M. (2007). Dynamic evolution of energetic outer zone electrons due to wave-particle interactions during storms. *Journal of Geophysical Research*, *112*, A10220. https://doi.org/10.1029/2007JA012368

Liu, K., Gary, S. P., & Winske, D. (2011). Excitation of magnetosonic waves in the terrestrial magnetosphere: Particle-in-cell simulations. *Journal of Geophysical Research*, *116*, A07212. https://doi.org/10.1029/2010JA016372

Liu, K., Winske, D., Gary, S. P., & Reeves, G. (2012). Relativistic electron scattering by large amplitude electromagnetic ion cyclotron waves: The role of phase bunching and trapping. *Journal of Geophysical Research*, *117*, A06218. https://doi.org/10.1029/2011JA017476

Millan, R. M., & Thorne, R. M. (2007). Review of radiation belt relativistic electron losses. *Journal of Atmospheric and Solar-Terrestrial Physics*, *69*(3), 362–377. https://doi.org/10.1016/j.jastp.2006.06.019

Omura, Y., Furuya, N., & Summers, D. (2007). Relativistic turning acceleration of resonant electrons by coherent whistler mode waves in a dipole magnetic field. *Journal of Geophysical Research*, *112*, A06236. https://doi.org/10.1029/2006JA012243

Omura, Y., & Summers, D. (2006). Dynamics of high-energy electrons interacting with whistler mode chorus emissions in the magnetosphere. *Journal of Geophysical Research*, *111*, A09222. https://doi.org/10.1029/2006JA011600

Shklyar, D., & Matsumoto, H. (2009). Oblique whistler-mode waves in the inhomogeneous magnetospheric plasma: Resonant interactions with energetic charged particles. *Surveys in Geophysics*, *30*(2), 55–104. https://doi.org/10.1007/s10712-009-9061-7

Shprits, Y. Y., Subbotin, D. A., Meredith, N. P., & Elkington, S. R. (2008). Review of modeling of losses and sources of relativistic electrons in the outer radiation belt II: Local acceleration and loss. *Journal of Atmospheric and Solar-Terrestrial Physics*, *70*(14), 1694–1713. https://doi.org/10.1016/j.jastp.2008.06.014

Summers, D. (2005). Quasi-linear diffusion coefficients for field-aligned electromagnetic waves with applications to the magnetosphere. *Journal of Geophysical Research*, *110*, A08213. https://doi.org/10.1029/2005JA011159

Summers, D., Thorne, R. M., & Xiao, F. (1998). Relativistic theory of wave-particle resonant diffusion with application to electron acceleration in the magnetosphere. *Journal of Geophysical Research*, *103*(A9), 20,487–20,500. https://doi.org/10.1029/98JA01740

Thorne, R. M. (2010). Radiation belt dynamics: The importance of wave-particle interactions. *Geophysical Research Letters*, *37*, L22107. https://doi.org/10.1029/2010GL044990

Thorne, R. M., Li, W., Ni, B., Ma, Q., Bortnik, J., Chen, L., et al. (2013). Rapid local acceleration of relativistic radiation-belt electrons by magnetospheric chorus. *Nature*, *504*(7480), 411–414. https://doi.org/10.1038/nature12889

Wilson, IIIL. B., Cattell, C., Kellogg, P., Wygant, J. R., Goetz, K., Breneman, A., & Kersten, K. (2011). The properties of large amplitude whistler mode waves in the magnetosphere: Propagation and relationship with geomagnetic activity. *Geophysical Research Letters*, *38*, L17107. https://doi.org/10.1029/2011GL048671

Wu, S., Denton, R. E., Liu, K., & Hudson, M. K. (2015). One- and two-dimensional hybrid simulations of whistler mode waves in a dipole field. *Journal of Geophysical Research: Space Physics*, *120*, 1908–1923. https://doi.org/10.1002/2014JA020736

Young, S. L., Denton, R. E., Anderson, B. J., & Hudson, M. K. (2002). Empirical model for μ scattering caused by field line curvature in a realistic magnetosphere. *Journal of Geophysical Research*, *107*(A6), 1069. https://doi.org/10.1029/2000JA000294

Zheng, Q., Zheng, Y., Fok, M.-C., & Lu, A. T. Y. (2012). Electron energy diffusion and advection due to non-linear electron-chorus wave interactions. *Journal of Atmospheric and Solar-Terrestrial Physics*, *80*, 152–160. https://doi.org/10.1016/j.jastp.2012.01.011